第 26 卷第 12 期 无 机 化 学 学 报 Vol.26 No.12
2010 年 12 月 CHINESE JOURNAL OF INORGANIC CHEMISTRY 2243-2250

$EuPO_4$:Zn@MCM-41 的制备和发光性质

曹 渊* 袁庆华 穆小静 徐彦芹 刘柏林
(重庆大学化学化工学院,重庆 400030)

摘要: 通过微波辅助水热法合成 MCM-41 介孔材料,经溶胶凝胶组装过程将 $EuPO_4$:Zn 分散到 MCM-41 表面上和孔道中,制备成以 MCM-41 为基质的复合发光材料 $EuPO_4$:Zn@MCM-41 粉末。通过 XRD、FTIR、氮吸附、SEM、HRTEM、EDS 对该材料进行了表征,用单因素法探究了原料配比($Eu(NO_3)_3$、$Zn(NO_3)_2$ 的加入量和反应条件(煅烧的温度、时间)对 $EuPO_4$:Zn@MCM-41 在 593 nm 处发光强度的影响,并研究其影响机理。荧光分析发现,$EuPO_4$:Zn 基本不发射荧光,而 $EuPO_4$:Zn@MCM-41 材料具有蓝光段和红光段的荧光发射,主要发光带以 468 和 593 nm 为中心。593 nm 处的发射归因于 Eu^{3+}的 4*f* 组内 $^5D_0 \rightarrow {}^7F_1$ 跃迁,即 Eu^{3+}中心离子所在晶格格位对称性决定的磁偶极跃迁。研究表明以 MCM-41 为载体,能够大大降低颗粒的团聚程度,并使 $EuPO_4$:Zn 颗粒具有更小的粒径; 同时 $EuPO_4$:Zn@MCM-41 中 Eu^{3+}发光中心具有更大的裂分,MCM-41 的纳米孔道使 Eu^{3+}的发光中心分离, 降低了 Eu^{3+}之间电子云之间的重叠,大大减小了荧光的猝灭,因此 MCM-41 能有效降低 Eu^{3+}复合物荧光猝灭。

关键词: MCM-41; Eu^{3+}复合物; 荧光; 制备
中图分类号: O657.34; O611.4 **文献标识码**: A **文章编号**: 1001-4861(2010)12-2243-08

Fabrication and Photoluminescence of $EuPO_4$:Zn@MCM-41 Composite

CAO Yuan* YUAN Qing-Hua MU Xiao-Jing XU Yan-Qin LIU Bo-Lin
(*Institute of Chemistry and Chemical Engineering, Chongqing University, Chongqing* 400030)

Abstract: MCM-41 was synthesized by microwave assisted hydro-thermal method. The $EuPO_4$:Zn@MCM-41 composite materials were obtained by doping the $EuPO_4$:Zn crystal onto the MCM-41 through a simple Pechini sol-gel process. The materials were characterized by XRD, N_2 adsorption/desorption, FTIR, SEM, TEM, EDS, and photoluminescence (PL) spectraoscopy. The PL spectra reveal that Pure $EuPO_4$:Zn powders do not show any PL emissions, however, $EuPO_4$:Zn@MCM-41 composites show strong blue (468 nm) and orange (593 nm) PL emissions. The main bands at 593 nm are ascribed to the $^5D_0$-$^7F_1$ transitions of Eu^{3+} and are the magnetic-dipole (M1) allowed transition, governed by the symmetry of the Eu^{3+} centers. The control factors for the PL intensity emitted at 593 nm were investigated by monofactorial analysis on prameters such as the amount of $Eu(NO_3)_3$ and $Zn(NO_3)_2$, the calcination temperature and calcination time. The PL results show that the dispersing effect of MCM-41 can decrease the agglomeration of $EuPO_4$:Zn particles thus making the particles smaller. Besides, larger splitting of Eu^{3+} centers and less overlapping of Eu^{3+} electron atmosphere are achieved by the MCM-41, suggesting that MCM-41 is an effective host for Eu^{3+} complexes for lowering the luminescence quenching effect.

Key words: MCM-41; Eu^{3+} complex; photoluminescence; fabrication

收稿日期:2010-06-07。收修改稿日期:2010-07-19。
中国博士后自然科学基金(No.20080440696)、211 工程第三期建设(No.S-09103)及中央高校基本科研业务费(No.CDJXS10221136)资助项目。
*通讯联系人。E-mail:caoyuan@cqu.edu.cn,Tel:+8602365111748
第一作者:曹 渊,男,47 岁,博士后,副教授;研究方向:介孔材料,生物材料。

The lanthanide compounds play a very important role in the luminescent materials, especially the compounds of Eu^{3+}[1-5]. If the particle of the luminescent materials is in nanometer range, there will be some special characters such as quantum confinement, electric, magnetic effects, making the luminescent materials much higher quantum yield[6]. However, the quantum yield of the luminescent materials was affected by the agglomeration of the powders, which quenches the PL sharply. In this respect, the problem about dispersion of the powders will be a critical issue. If suitable inorganic host materials with good thermal properties as well as chemical stability are found, the problem of the powders′ dispersion will be resolved properly. The MCM-41 mesoporous molecular sieves[7-8] with the pore size ranged from 2 to 10 nm have high specific surface area, good thermal properties, and chemical stability. Recently, some applications in carriers for luminescent materials have been reported[9-13]. The Eu^{3+} complexes encapsulated in MCM-41 have extensive applications, such as drug release[14]. Besides, it can be used as sensors for gas or fluid, or used to make the electronic equipment, as well as the amplification in the dye laser[15].

We report here the synthesis of MCM-41 by microwave assisted hydro-thermal method and the roles of MCM-41 played in fabrication of composite materials $EuPO_4$:Zn@MCM-41. The obtained composite materials emit both blue and orange fluorescence.

1 Experimental

1.1 Preparation of MCM-41

The MCM-41 was synthesized by microwave assisted hydro-thermal method. First, cetyltrimenthylammonnium bromide (CTAB, 0.6 g) was dissolved into water (250 mL) and stirred for 10 min, then 3.5 mL 2 mol·L^{-1} NaOH was added and stirred for 10 min. Then, 2.5 mL of tetraethoxysilane (TEOS) was added into the solution with vigorous stirring for 1 hour. The mixture was loaded into microwave oven (TCMC-204) and heated for 1 hour under 120 W. The resultant solid was filtered and then rinsed with deionized water. Then it was dried at 80 ℃ for 5 h. To remove the surfactants, the synthesized material was heated at 550 ℃ for 5 h. The obtained MCM-41 was denoted as A.

1.2 Fabrication of $EuPO_4$:Zn@MCM-41

The $EuPO_4$:Zn@MCM-41 composites were synthesized according to the literature with some modification[15]. 1 mmol $EuNO_3 \cdot 6H_2O$ and 2 mmol $Zn(NO_3)_2 \cdot 6H_2O$ were dissolved in 5 mL distilled water. Then 2 mmol $(NH_4)_2HPO_4$ was added into the above mixture and the white sediment was observed. 20 mL of water-ethanol (V/V=15∶5) solution with 0.840 6 g of citric acid was used as a chelating agent for the metal ions. Polyethylene glycol was added as a cross-linking agent with a concentration of 0.20 g·mL^{-1}. The solution was stirred for 1 h to form a sol, and then the MCM-41 powder (A) was added with stirring. The suspension was further stirred for another 3 h, and then the final particles were separated by centrifugation. After that, the samples were immediately dried at 100 ℃ for 1 h. Then the dried samples were heated to 800 ℃ with a heating rate of 20 ℃·min^{-1}, and held at this temperature for 5 h. The composite material of $EuPO_4$:Zn@MCM-41 (B) was obtained.

1.3 Fabrication of pure $EuPO_4$:Zn

For the purpose of comparison, the $EuPO_4$:Zn was fabricated in a similar process to produce $EuPO_4$∶Zn@MCM-41powder. However, there was no need to add the powder of MCM-41 in the sol Eu^{3+}. Then the composite sol (C) was annealed in the same process.

1.4 Characterization

Wide-angle XRD data (D/MAX-Ⅲ CX) were recorded, using nickel-filtered Cu $K\alpha$ radiation (λ = 0.154 18 nm) with a scan speed of 2°·min^{-1}. The N_2 adsorption/desorption isotherms were measured at −198.938 ℃ in the relative pressure range of 0.0~1.0 using a Micromeritics on the volumetric adsorption analyzer (ASAP 2 020 V 3.01 H). The specific surface area was calculated by Brunauer-Emmett-Teller (BET) analysis, pore size and volume was estimated using Barret-Joner-Halenda (BJH) model. TEM (JEOL JEM-2010) at 200 kV was used to examine particle size and shape of samples. SEM (FEI SIRION100) observation was carried out at operating voltages varying from 1.0 to 30.0 kV. Elemental analysis was performed using an

energy-dispersive spectrometer (EDS) attached to TEM instrument. The fluorescence experiments were carried out on a RF-5301PC spectrometer. The slit width was 5 nm, and excitation and emission wavelengths were 394 nm and 593 nm.

2 Results and discussion

2.1 XRD analysis

The powder XRD pattern for MCM-41 was illustrated in Fig.1(a). The diffraction patterns clearly exhibits the characteristic diffraction peaks ((100) 2θ= 2.76°), ((110), 2θ=4.60°), and ((200), 2θ=5.26°), reflecting the typically hexagonal structure regularity of MCM-41, in agreement with the literature report[16]. The cell parameter $a_0=2d_{100}/\sqrt{3}$, a_0=3.69 nm. The composites B also show the characteristic diffraction peak (100), however, the (110) and (200) peaks disappear under 800 ℃ suggesting that the order of the MCM-41 decreases a little. Compared to A and B, there are not any observable diffraction peaks from C. Wide-angle XRD (2°~80°) patterns for A, B, C, and the standard data of $EuPO_4$ as a reference (PDF No.83-0654) are illustrated in Fig.1(b). The characteristic diffractions of $EuPO_4$ crystal (PDF No. 83-0654) also are observed in sample C, indicating that a pure phase of $EuPO_4$ has already formed. The EDS analysis was performed on the B composites, and the contents of all the elements are shown in Table 1. The results show that the molar content of Eu, Zn and P is 9.44%, 0.37% and 9.80%, respectively. The XRD results indicate that the stoichiometry is 9.44%:9.44% for all Eu^{3+} with PO_4^{3-} and the main crystalline phase is $EuPO_4$. The residual PO_4^{3-} in the $EuPO_4$ crystal is 0.36% which could be coordinated with 0.37% of Zn^{2+}, however, the diffractions of $Zn_2P_2O_7$ or ZnO are not detected. The new synthesized composites are denoted as $EuPO_4$:Zn@MCM-41. Fig.1(b) also shows the characteristic diffractions of sample A and C in B, suggesting the $EuPO_4$:Zn has been loaded on the surface or in channel of MCM-41.

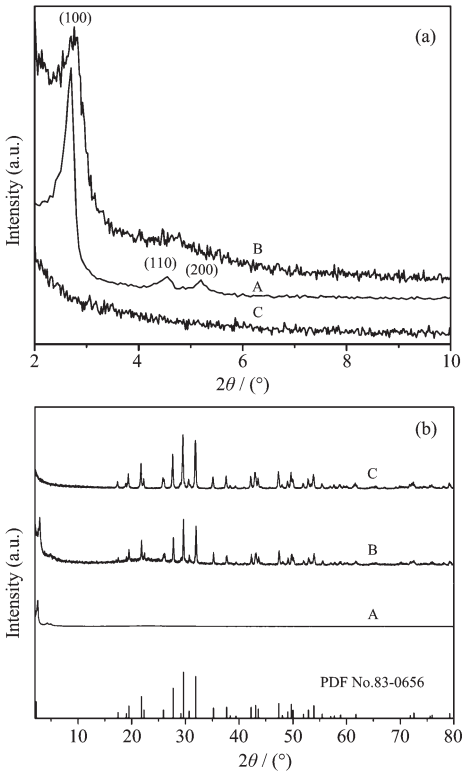

Fig.1　Low-angle XRD patterns and wide-angle XRD patterns for A, B and C

Table 1　Molar content in the composite of $EuPO_4$:Zn@MCM-41 by EDS

Element	Peak area	Weight / %	Atom / %
O	3 367	30.92	62.98
Si	2 958	15.01	17.41
P	1 852	9.32	9.80
Zn	102	0.74	0.37
Eu	4 191	44.02	9.44

2.2 N_2 adsorption/desorption and FTIR analysis

The respective adsorption/desorption isotherms of A and B are shown in Fig.2. Both A and B show typical Ⅳ isotherms H1-hysteresis with p/p_0 of 0.0 to 1.0, characteristic of mesoporous silicate material. The volume of A is nearly twice of B suggesting that small size $EuPO_4$:Zn particles are encapsulated in the pores of

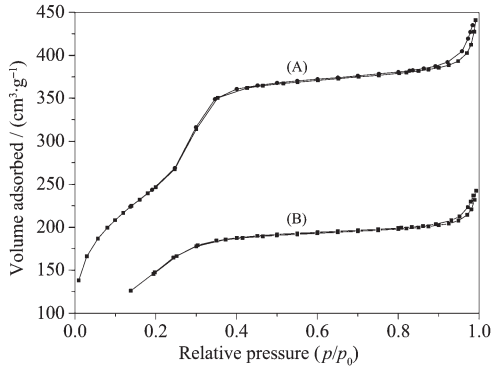

Fig.2　N_2 adsorption/desorption isotherms of A and B

A. The corresponding pore sizes calculated from the absorption branch of N_2 adsorption/desorption isotherms are shown in Table 2.

Table 2 Parameters of N_2 adsorption/desorption isotherms for A and B

Sample	Pore volume / ($cm^3 \cdot g^{-1}$)	Pore size / nm	BET surface area / ($m^2 \cdot g^{-1}$)
A	0.676	3.113	956
B	0.369	3.015	586

Fig.3 shows FTIR spectra of A and B. The rather broad band centered at 3 460 cm^{-1} is due to adsorbed or hydrogen-bonded water molecules[17]. The peak at 1 640 cm^{-1} can be attributed to the flexion vibration of O-H groups of water molecules. The bands at 1 080, 803, 465 cm^{-1} are antisymmetry, symmetry stretching vibrations, and bending vibration of the mesoporous frame work (Si-O-Si) bridges, respectively[18]. Compared with A, five new peaks (1 773, 1 342, 1 230, 570 cm^{-1}) appear in B due to the lattice vibration of PO_4^{3-}. The peaks both at 962 and 551 cm^{-1} become much sharper than A, which may be due to the weaker symmetrical stretching vibration of OH bonds in the pore affected by encapsulating. Similarly, the -OH flexion vibration shifts from 1 640 to 1 617 cm^{-1}, in agreement with the result of XRD.

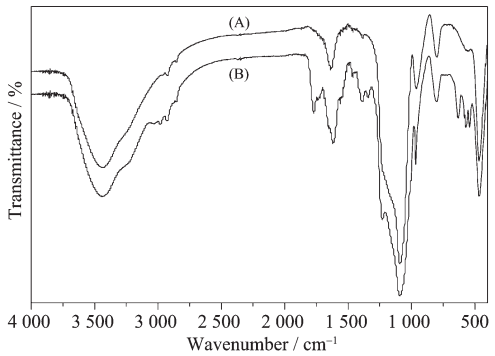

Fig.3 FTIR for A and B

2.3 SEM and TEM analysis

SEM and TEM images for A, B, and C are shown in Fig.4. As shown in SA, the particles for sample A are unified rod-shape with an average particle diameter of 150 nm. The particles for sample C show agglomeration seriously with particle diameter larger than 60 nm. However, the SEM image for particles B are unified rod-shape like sample A. The TEM image for B (TB) reveals that the $EuPO_4$:Zn particles (black) are dispersed on MCM-41, due to an electrostatic adsorption on the Si-OH groups on the surface of MCM-41[19]. Hsieh et al.[20] found that it is the electrostatic force induced by the charged oxygen defects that makes the metal nanoparticles strongly attracted.

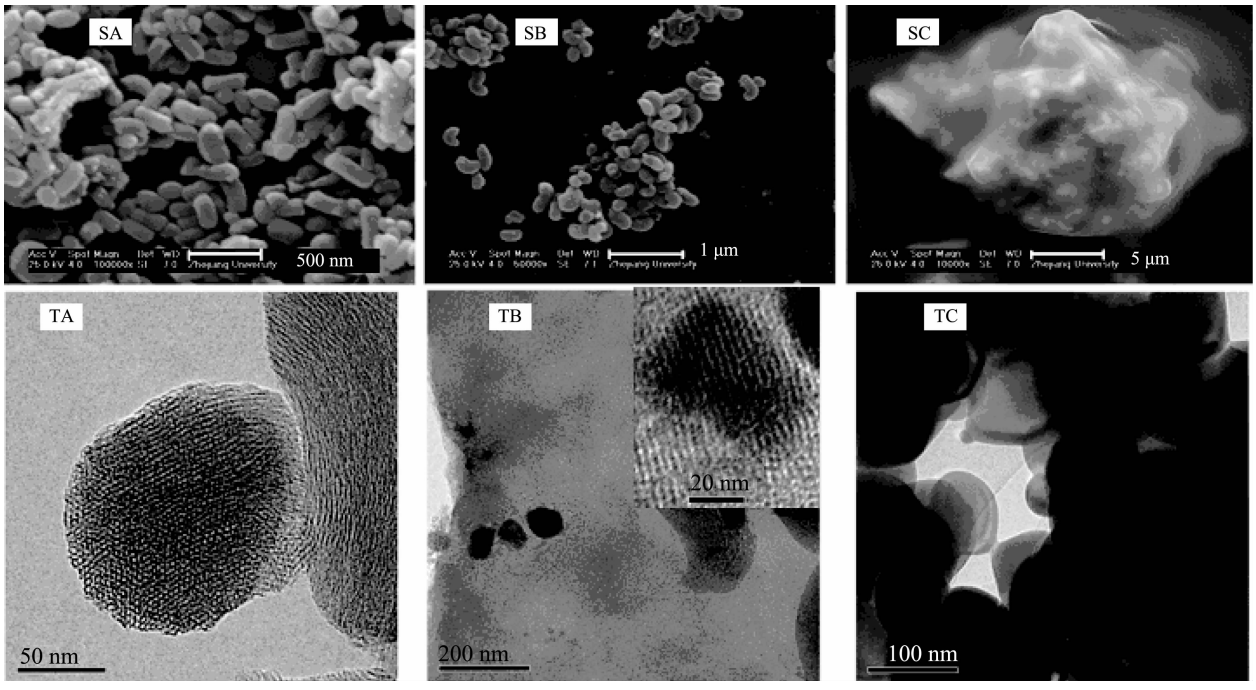

Fig.4 SEM images for A, B and C (respectively SA, SB and SC); TEM images for A, B and C (TA, TB and TC)

2.4 Fluorescence spectra

The PL spectra for A, B, and C are illustrated in Fig.5. In Fig.5a, the strongest excitation band of B is centered at 394 nm and there are not any detectable absorption bands for C. In Fig.5b, the PL emission spectrum of B not only shows the bands (430~490 nm) appeared in MCM-41 originated from structural defects, such as non-bridging oxygen hole centers (NBOHCs), ≡Si-O·, oxygen-deficient centers[21], but also has characteristic bands of Eu^{3+}, including 587, 593, 612 nm. The main bands (587 nm and 593 nm) ascribe to the $^5D_0$-$^7F_1$ transitions of Eu^{3+} and are the magnetic-dipole (M1) allowed transition, decided by the symmetry of the Eu^{3+} centers. Usually, the $^5D_0$-$^7F_1$ transitions are weaker than the $^5D_0$-$^7F_2$ ones which are forced electric-dipole (E1) transitions as reported in literatures[9,15]. The Eu^{3+} ions in B are at the sites of symmetry inversion centers sensitive to the symmetry than the environment of the coordination[22]. Compared to B, sample C does not show any detectable fluorescence, suggesting that the observed emission arise from the encapsulation of the $EuPO_4$:Zn in MCM-41. Because the PL quenching effect of characteristic emission decreases with the agglomeration, the characteristic emissions (band at 587 nm and 593 nm) of B can be attributed to the matrix of MCM-41 because of the large surface and small volume which can disparate the $EuPO_4$:Zn particles well. Besides, the small particles of $EuPO_4$:Zn in the pores of MCM-41 also contributed to the PL characteristic emission of Eu^{3+}.

Fig.6 shows optical micrographs for A, B and C, recorded by a digitalized inverted microscope. All the samples are observed in the fluorescence mode (excitation with Hg lamp at violet radiation). The blue emission can be observed obviously in A, and there is not visible radiation observed in C. However, both the blue and orange light are observed in B, agreed with the results of fluorescence spectra.

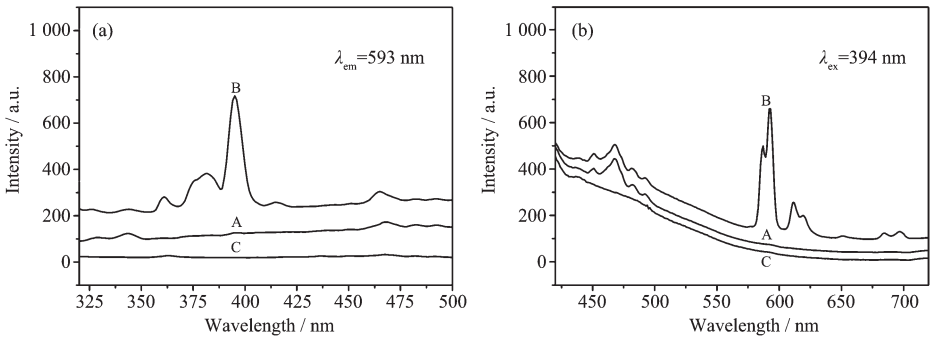

Fig.5　PL excitation spectra (a) and the PL emission spectra (b) for A, B and C

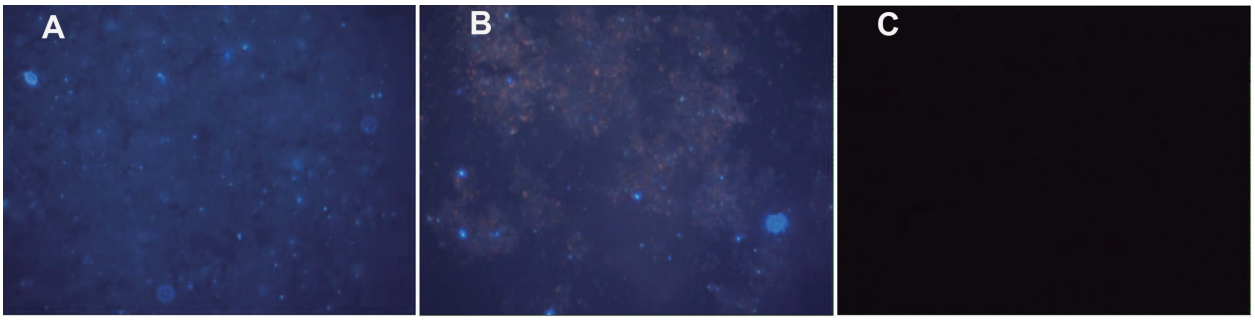

Fig.6　Optical micrographs for A, B and C, magnification of 40× (A) and 40× (B), 40× (C)

2.5 Adding amount of the Eu and Zn of the composite B

In general, the excess of activators quenches the photoluminescence. So, it is necessary to find the critical concentration of Eu^{3+} in terms of optimizing the luminous efficiency of the composite B. Because of the constant contents of MCM-41 in B, the relative values of PL intensity (I_{593}:I_{468}) are used to measure the Eu^{3+} PL intensity for the composite and the PL intensity emitted at 468 nm is used as the internal standard for B. The PL

emission spectra and the relative value of I_{593}:I_{468} are affected by the adding amount of $EuNO_3 \cdot 6H_2O$ as illustrated in Fig.7 under the condition of 2 mmol $Zn(NO_3)_2 \cdot 6H_2O$. As seen from b, the relative value of I_{593}:I_{468} increases at first, then decreases with the increase of the adding amount of $EuNO_3 \cdot 6H_2O$. This is due to that the PL intensity of Eu^{3+} ions have relationship with the density of Eu^{3+} ions in elementary cell[23]. When the adding amount of $EuNO_3 \cdot 6H_2O$ is less than 1 mmol, the molar content of Eu in B is less than 9.44% and the density of Eu^{3+} ions in the cell is increased with the adding amount of $EuNO_3 \cdot 6H_2O$, leading to the increase of PL intensity of Eu^{3+}. Furthermore, when the adding amount of $EuNO_3 \cdot 6H_2O$ is 1 mmol, the molar content of Eu in B is 9.44% and the Eu^{3+} ions could be coordinated with 9.44% of PO_4^{3-} ions completely. As the consequence, the PL intensity of Eu^{3+} ions reaches the strongest. However, with the further increase in the adding amount of $EuNO_3 \cdot 6H_2O$, the increased Eu^{3+} ions in the $EuPO_4$ crystalline phase may lead to the shorter distance between the Eu^{3+} ions centers. Besides, the superposition of Eu^{3+} electron cloud becomes more seriously, thus decreasing the PL emission at 593 nm. So, the appropriate amount of $EuNO_3 \cdot 6H_2O$ is 1 mmol.

The PL emission spectra and the trend chart affected by adding amount of $Zn(NO_3)_2 \cdot 6H_2O$ are illustrated in Fig.8 under the condition of 1 mmol $EuNO_3 \cdot 6H_2O$. In b, the relative value of I_{593}:I_{468} increases sharply until the adding amount of $Zn(NO_3)_2 \cdot 6H_2O$ reaches to 2 mmol. However, the value decreases with the further increase of the $Zn(NO_3)_2 \cdot 6H_2O$. The Zn^{2+} may be regarded as the taps in the lattice of europium[24] to capture the photons, and the electrons would transfer to excited state of Eu^{3+} finally via way of $Zn^{2+} \rightarrow PO_4^{3-} \rightarrow Eu^{3+}$. As a result, the PL emission of Eu^{3+} becomes much stronger. However, the sequential increase of adding amount of $Zn(NO_3)_2 \cdot 6H_2O$ induced to the molar content of Zn in the B comosite more than 0.37%. The less than 0.36% P molar content is not enough to coordinate with Zn^{2+} ions by PO_4^{3-} ions. On the contrast, the interaction between the Zn^{2+} ions and Eu^{3+} ions becomes stronger, leading to

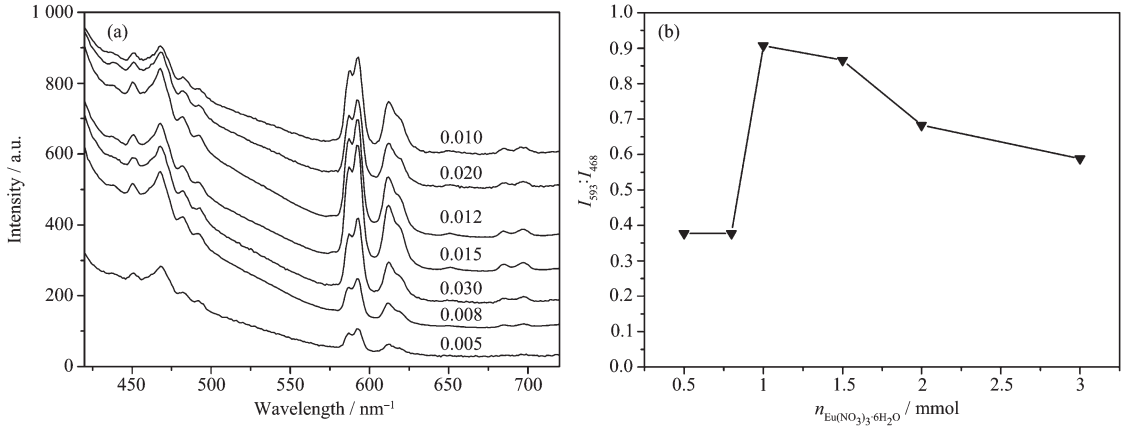

Fig.7 PL spectra (a) and the value of I_{593}:I_{468} changed with the content of $EuNO_3 \cdot 6H_2O$

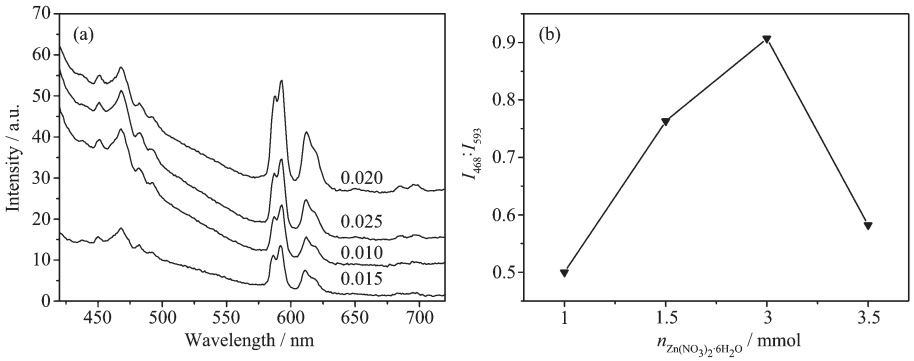

Fig.8 PL spectra (a) and the value of I_{593}:I_{468} as a function of $Zn(NO_3)_2 \cdot 6H_2O$ content

the energy of some excited state europium lower than the energy $^5D_0 \rightarrow {}^7F_1$ transi-tion in $4f$[24]. So the PL intensity becomes much weaker, and the appropriate amount of $Zn(NO_3)_2 \cdot 6H_2O$ is 2 mmol.

2.6 Calcination conditions

The relative value of $I_{593}:I_{468}$ heated at different temperatures are illustrated in Fig.9(a). The relative value increases with temperature and the maximum is obtained at 800 ℃. High temperature is beneficial to the formation of crystal[22], so the $EuPO_4$:Zn crystalline phase is formed perfectly at 800 ℃. However, the relative value decreases greatly at 900 ℃, due to the collapse of MCM-41 and poor dispersion of $EuPO_4$:Zn particles. The XRD patterns obtained at different temperatures are illustrated in b. The strongest characteristic diffractions for B were obtained at 800 ℃ in accord with results in Fig.9(a), suggesting well formation of the lattice arrangement. So the reasonable calcination temperature is 800 ℃.

The PL emission spectra under 800 ℃ as the function of the calcination time and the relative value of $I_{593}:I_{468}$ are illustrated in Fig.10. In b, there is a sharp increase in the relative value from calcination time of 2 to 3 h, then increases slowly with the calcination time. The emission at 593 nm is decided by the symmetry inversion centers of Eu^{3+}, so longer calcination time is favorable to better arrangement of crystal phase,thus stronger PL emission.

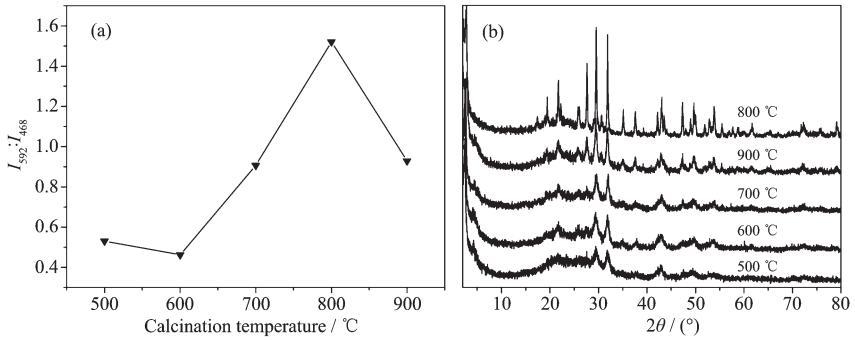

Fig.9　Relative value of $I_{593}:I_{468}$ and XRD patterns as a function of calcination temperature

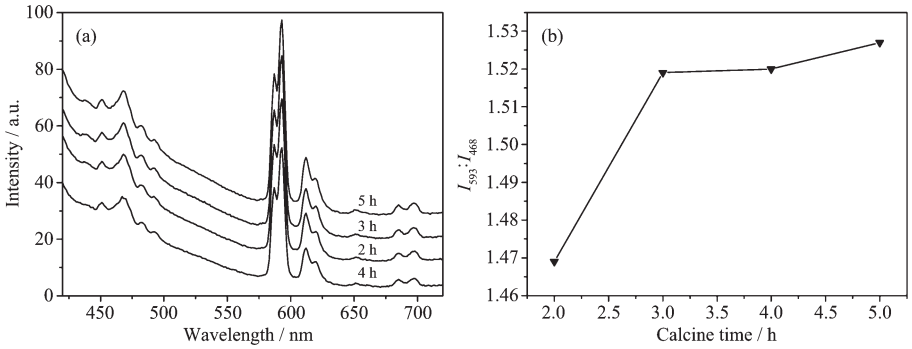

Fig.10　PL spectra (a) and the relative value of $I_{593}:I_{468}$

3 Conclusions

The $EuPO_4$:Zn@MCM-41 composite was synthesized by dispersing the $EuPO_4$:Zn particles onto the MCM-41 through a simple Pechini sol-gel process. The $EuPO_4$:Zn particles were dispersed well by the host of MCM-41 compared to the pure $EuPO_4$:Zn. Besides, the $EuPO_4$:Zn@MCM-41 shows both the blue and orange PL emissions, which is the magnetic-dipole allowed transition (M1) ascribed to the $^5D_0$-$^7F_1$ transitions of Eu^{3+} ions. The highest PL emission at 593 nm for $EuPO_4$:Zn @MCM-41 composite has been evaluated by the mono-factorial analysis. The Zn^{2+} in the $EuPO_4$:Zn@MCM-41 composite may be considered as the taps in the lattice of europium to capture the photons, and the electrons would transfer to the excited stated of Eu^{3+} via way of $Zn^{2+} \rightarrow PO_4^{3-} \rightarrow Eu^{3+}$.

The dispersion effect of MCM-41 is confirmed. Moreover, this paper suggests no more than enough the

expensive rare earth should be used. Under optimized conditions, the $EuPO_4$:Zn@MCM-41 can be used as a luminescent material in solid-state light resources.

References:

[1] Kuo T W, Chen T M, Mou. *J. Lumin.*, **2010**,**130**:483-487

[2] Tian L, Yang P, Wu H, et al. *J. Lumin.*, **2010**,**130**:717-721

[3] Yu Y, Chen D, Huang P, et al. *Ceram. Int.*, **2010**,**136**:1091-1094

[4] Yaiphaba N, Ningthoujam R S, Shanta Singh N, et al. *J. Lumin.*, **2010**,**130**:174-180

[5] Chaliha R S, Annapurna K, Tarafder A, et al. *J. Solid State Chem.*, **2009**,**11**:1325-1332

[6] Ronda C R. *J. Lumin.*, **1997**,**72-74**:49-54

[7] Beck S, Vartuli J C, Roth W J, et al. *J. Am. Chem. Soc.*, **1992**,**114**:10834-10843

[8] Kresge C T, Leonowicz M E, Roth W J, et al. *Nature*, **1992**, **359**:710-712

[9] Yan B, Zhou B. *J. Photochem. Photobiol., A*, **2008**,**195**:314-322

[10]Sun L N, Yu J B, Zhang H J, et al. *Micropor. Mesopor. Mater.*, **2007**,**98**:156-165

[11]Bruno S M, Ferreira Sá R A, Carlos L D, et al. *Micropor. Mesopor. Mater.*, **2008**,**113**:453-462

[12]Li Y, Yan B. *J. Solid State Chem.*, **2008**,**181**:1032-1039

[13]Garcia F A C, Silva J C M, Filho G N R, et al. *Micropor. Mesopor. Mater.*, **2008**,**113**:562-574

[14]Yang P P, Quan Z W, Li J, et al. *Micropor. Mesopor. Mater.*, **2008**,**116**:524-531

[15]Yang P P, Quan Z W, Lin J, et al. *Biomaterials*, **2008**,**29**:692-702

[16]Li Y, Yan B. *Micropor. Mesopor. Mater.*, **2010**,**128**:62-70

[17]Ojeda M L, Campero A, López-Cortés J G, et al. *J. Mol. Catal., A: Chem.*, **2008**,**281**:137-145

[18]Jiang T, Tang Y, Zhao Q, et al. *Colloids Surf., A*, **2008**,**315**: 299-303

[19]Wang P, Zhu Y, Yang X, et al. *Acta Mater.*, **2008**,**56**:1144-1150

[20]Hsieh Y P, Chen J W, Liang C T, et al. *J. Lumin.*, **2008**,**128**: 553-558

[21]Li X X, Tang Y H, Lin L W, et al. *Micropor. Mesopor. Mater.*, **2008**,**111**:591-595

[22]Maia A S, Stefani R, Kodaira C A, et al. *Opt. Mater.*, **2008**,**31**: 440-444

[23]Schmechel R, Winkler H, Xaomao L, et al. *Scripta Mater.*, **2001**,**44**:1213-1217

[24]Ryu H, Bartwal K S. *J. Alloys Compd.*, **2008**,**461**:395-398